ACS OMEGA

Open Access

http://pubs.acs.org/journal/acsodf

Article

Aspect Ratio Modulation of Sucralose through {002}/{011} Preferred Orientation in Antisolvent Crystallization

Qiaoyan Xu, Zhoulin Lv, Xiaoping Chen, Shaoheng Li, Changqi Huang, Jingjing Chen, Yingshu Wang,* Haohong Li, and Huidong Zheng*

Cite This: *ACS Omega* 2023, 8, 41145−41155

Read Online

ACCESS | Metrics & More | Article Recommendations | Supporting Information

ABSTRACT: The aspect ratio modulation in the alcoholysis process is highly significant for the production of high-quality sucralose. In this work, antisolvent crystallization (ASC) accompanied by preferred orientation was first adopted in the sucralose separation, based on which simultaneous modulations on aspect ratio, solubility, and stability have been realized. In detail, after the alcoholysis process in methanol, four antisolvents bearing different functional groups were used in ASC, i.e., isopentanol (IPN), isovaleraldehyde (IVD), isovaleric acid (IVA), and isobutyl propionate (IBP). To our interest, when IVA was used as the antisolvent, the highest separation efficiency (49.33%), fastest crystallizing rate (5.64%/h), lowest aspect ratio (1.55), and solubility (9.28 wt %) and good thermal stability (131.65 °C) of sucralose were achieved. Single crystal structures of sucralose using different antisolvents have been determined. Sucralose using IVA as the antisolvent exhibits the greatest molecular distortion and strongest intermolecular C−H···Cl hydrogen bonds; thus, the preferred growth along {002}/{011} directions has occurred and accounted for its lower aspect ratio, worse solubility, and better stability. The strongest methanol···IVA interactions due to the presence of a carboxyl group can accelerate the formation of the emulsion, resulting in the fastest crystallizing rate. The antisolvent screening and the discovery about relative mechanisms will provide a theoretical guide for the production of high-quality sucralose.

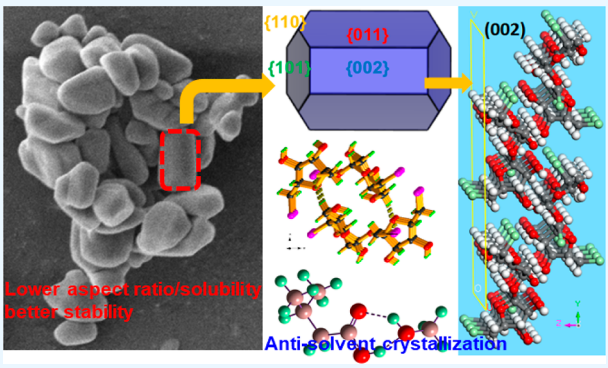

1. INTRODUCTION

As a new generation of artificial sweetener, sucralose (Scheme 1) has been widely used in food and pharmaceuticals because it is highly sweet, non-nutritive, noncariogenic, and biologically safe.[1,2] For example, it is very appropriate for people suffering from diabetes or obesity.[3] It has shown attractive commercial prospects, whose global market consumption has reached about 20,000 tons (5 billion RMB) in 2022. In the mainstream monogroup protection production process, sucralose was synthesized by selectively substituting three hydroxyl groups of sucrose with chlorine atoms through three steps: protection of 6-hydroxyl by acylation to give sucrose-6-acetate (SA-6), then selective chlorination on SA-6 to generate 4,1′,6′-trichlorosucrose-6-acetate, and finally, alcoholysis to obtain the product (Scheme S1).[4] Although this approach can be executed under mild conditions, the overall yield is low (about 40%) because there are many byproducts in each step due to similar hydroxyl activities and intramolecular acetyl transfer.[5] For example, after the alcoholysis reaction, there are 10 byproducts (bis- or monochloro products, Scheme S2), which must be removed by tedious processes such as multiextraction and recrystallization. The low separation efficiency and unsatisfied purity have puzzled the researchers for a long time.[6] Besides, morphology (including crystal shape and aspect ratio) can determine its properties, for example, flowability, solubility, drying, and compression. In order to produce high-quality sucralose product, the following issues must be

Scheme 1. Molecular Structures of Sucralose and Antisolvents Used in This Work

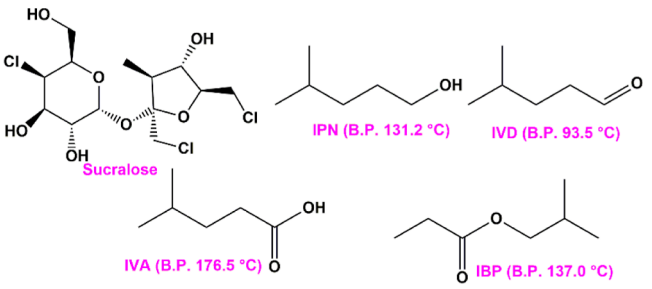

Received: June 1, 2023
Accepted: October 2, 2023
Published: October 24, 2023

improved: (1) the poor flowability led by high aspect ratio has limited its further application,[7] how to obtain globular products with lower aspect ratio is challengeable; (2) the sweetness of sucralose can be closely relative to the solubility because the hydration structure may enhance the sucralose−protein interaction via hydrogen bonds.[8,9] The solubility modulation is meaningful for its special application such as food additives; (3) sucralose could be degraded at elevated temperature with the generation of hazardous polychlorinated aromatic hydrocarbons.[10] The enhancement of thermal stability will be very beneficial for its postprocessing. Therefore, the simultaneous modulations of aspect ratio, solubility, and stability of sucralose in the final alcoholysis process seem highly significant for the sucralose production.

Antisolvent crystallization (ASC) is a powerful method for recrystallization/purification in pharmaceutical and material industries, which can overcome the disadvantages of natural crystallization (low efficiency and large energy loss).[11,12] In the ASC, by the simple addition of an antisolvent bearing poor solubility for the target solute, the solutes can be solidified into crystals with various polymorphs.[13] More importantly, the proper choice of antisolvent can modulate the nucleation and growth of solute, which provides efficient strategy for morphology and property control.[14,15] In detail, the antisolvent could affect the solute crystallization by serving as a surfactant to induce preferential growth in a specific direction.[16−18] Herein, the molecular characteristics of antisolvent (such as polarity or functionality) are key to product morphologies. Consequently, the crystals of target solute can oppose different intermolecular interaction strength and modes, resulting in various physical properties such as solubility and stability.[19] Recently, Choi et al. reported that the nucleation of the ASC process can be determined by emulsion particles, which were generated during mixing two miscible solvents.[20] Huang et al. investigated the effects of temperature, stirring rate, supersaturation, and ultrasonic power on the antisolvent crystallization of sucrose.[21] Xie et al. conducted a study about the effect of solvents on sucralose crystal morphology in water, methanol, and ethanol.[22] However, up to now, ASC has never been adopted in the sucralose. In this work, four antisolvents, i.e., isopentanol (IPN), isovaleraldehyde (IVD), isovaleric acid (IVA), and isobutyl propionate (IBP) bearing methyl side group and different functional groups (hydroxyl, formyl, carboxyl, and ester) have been adopted in the ASC of sucralose (Scheme 1). The side groups will make the packing looser during the formation of emulsion with methanol, which could provide more space for the encapsulation of solute molecules for further aggregation. Consequently, aspect ratio, solubilities, and stabilities of four sucralose products have been investigated. To our interest, when IVA was used as the antisolvent, the highest separation efficiency, lowest aspect ratio, lowest solubility, and best stability can be achieved. The relative mechanism was discussed based on the single crystal structural analysis. This work will provide a theoretical guide for the production of high-quality sucralose.

2. EXPERIMENTAL SECTION

2.1. Materials and Physical Measurements. High-purity sucralose was provided by Sanming Techno Food Ingredients Co., Ltd., whose purity has been validated by HPLC (Figure S1a). This sucralose was further used as seed crystals in the ASC process. Other chemicals including IPN, IVD, IVA, IBP, methylisobutyl ketone (MIBK), methanol, acetonitrile, acetone, *N*-methyl pyrrolidone, methylisopropyl ketone, and NaOH were all AR grade and purchased from Shanghai Micklin Co., Ltd. All of these reagents were used without further purification. NKC-9 ion-exchange resin was obtained from NTU Synthetic Chemistry.

IR spectra were recorded on a Thermo Scientific Nicolet iS50 spectrophotometer (4000−500 cm^{-1}) using the ATR model. Elemental analyses for C, H, and N were performed on a Vario MICRO elemental analyzer. Powder XRD patterns at room temperatures and 60 °C were obtained using a RIGAKU Ultima IV diffractometer equipped with temperature controller under Cu Kα radiation (λ = 1.54056 Å) in the range of 5−50°. The SEM images and the size distributions were determined on a Nova NanoSEM 230 field-emission scanning electron microscope. The thermal stabilities were determined by TGA-DSC on a METTLER-TOLEDO/DSC 3 in the temperature of 30−200 °C under a nitrogen atmosphere. ^{1}H NMR spectra were recorded on a JNM-ECZ500R in C_2D_3N, whose chemical shifts were reported in parts per million (ppm) downfield from tetramethylsilane. X-ray diffraction single crystal structural determinations were carried out on a Bruker Apex Duo2 CCD area diffractometer.

The quantitative analysis of sucralose was executed on high-performance liquid chromatography (HPLC) equipped with a refractive index detector (RID) (shimadzuRID-10A) and Phenomenex Luna C18 (4.6 mm × 250 mm × 5 μm) detector (Waters Alliance e2695). The purity of sucralose was determined by area normalization method. According to relative literature, the measurement parameters of HPLC were set as follows:[23] gas speed in nebulizer: 2.12 L/min, temperature of floating tube: 90 °C, mobile phase: water and acetonitrile with ratio of 8:2 (v/v), column temperature: 40 °C, flow rate: 1.0 mL/min. The content of sucralose was estimated by external standard method, in which the parameters of RID were set as follows: mobile phase: methanol/acetonitrile/water (1:1:3, v/v), column temperature: 40 °C, and flow rate: 1.0 mL/min.

2.2. Synthesis. The 95% sucralose was similar to the components of alcoholysis products, which was self-prepared through three-step reaction using sucrose as starting materials according to literature (Scheme S1).[4] The crude sucralose solution was prepared as follows:[24,25] 75% 4,1′,6′-trichlorosucrose-6-acetate (30.0 g) was dissolved in 114 mL of methanol. In another flask, the NaOH methanol solution with a concentration of 0.7869 mol/L was prepared, which was used as an alcoholysis catalyst. 7.8 mL of catalyst was added dropwise into the sucralose solution and kept reacting for 2 h at 40 °C. Afterward, the NKC-9 ion-exchange resin was added to quench the reaction. The mixture was kept at 30 °C for another 0.5 h after the pH value was adjusted to be neutral. Ion exchange resin was filtered, and methanol was removed by vacuum evaporation. The raw product was dried at 50 °C under 0.1 MPa to obtain pale yellow solids (25.0 g, yield: 83.40%).

2.3. Antisolvent Crystallization Process. Raw sucralose (purity: 95%) was used in the antisolvent crystallization (ASC) process because it is closer to industrial conditions. In detail, the as-synthesized 95% sucralose (2.1899 g) was dissolved in 6.6 mL of methanol (0.1568 mol) at 30 °C and then equimolar antisolvents (IPN, IVD, IVA, and IBP) were added with one-time mode under magnetic stirring conditions at a rate of 1300 rpm/min; in the meantime, seed crystals (0.0794 g) were thrown in. The sucralose solids can crystallize gradually. The

https://doi.org/10.1021/acsomega.3c03877
ACS Omega 2023, 8, 41145−41155

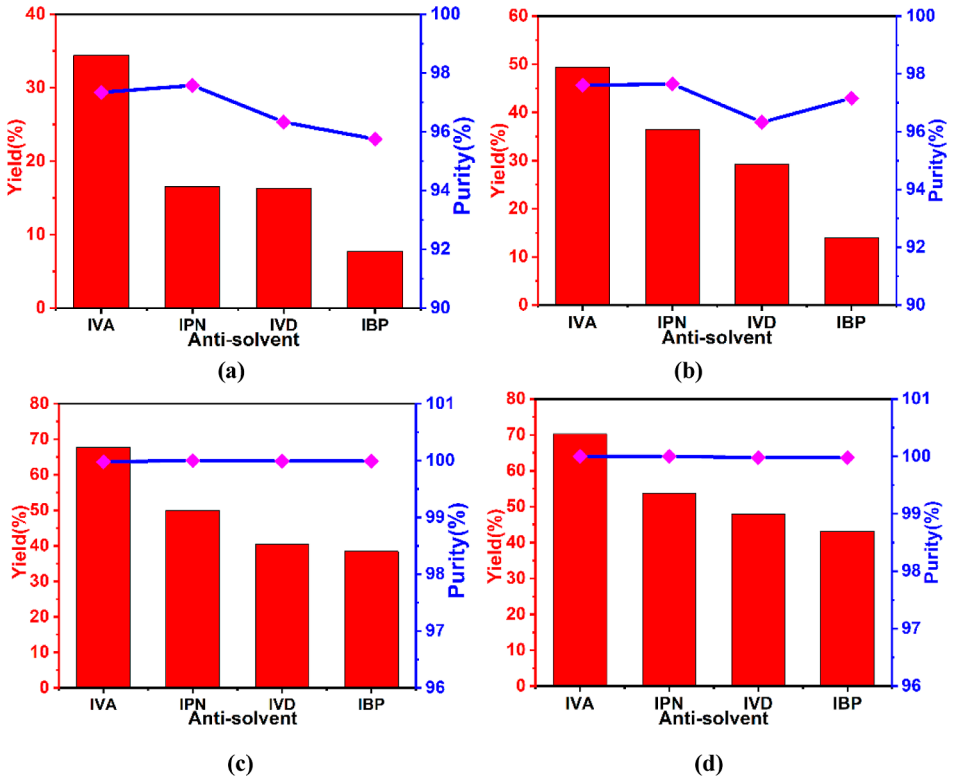

Figure 1. Antisolvent crystallization yields and purities: (a) at 24 h and (b) at 48 h using raw sucralose (95%) as starting material; (c) at 24 h and (d) at 48 h using high-purity sucralose as starting material.

crystallization in water was conducted under the same conditions, and the yield and purity were determined at the crystallization time of 48 h. By extracting suspension samples at interval of 24 and 48 h, the product purities were determined by area normalization method in HPLC of crystals, and the yields (Y) were calculated according to the following equation, in which C_0 is the initial concentration of sucralose, and C_i is the residue concentration in mother liquors

$$Y_{\text{sucralose}} = \frac{C_0 - C_i}{C_0} \times 100\%$$

In the crystallization rate measurements, in order to rule out the effect of impurities, high purity sucralose was used as starting materials. All the conditions were the same as the above antisolvent crystallization experiments. In order to discuss the effect of different functional groups on antisolvent (hydroxyl, formyl, carboxyl, and ester groups), equimolar IPN, IVD, IVA, IBP, and MIBK were added. The suspension samples were taken at 0.25, 0.5, 0.75, 1, 1.5, 2, 4, 6, 12, 24, 36, and 48 h. The crystallization rate was estimated by determining the residue sucralose in the mother liquor.

2.4. Solubility Measurements. The solubility was measured by the isothermal method.[26] In a jacked glass vessel, the methanol/antisolvent mixed solvents with series of molar ratio (0.1−1.0) were prepared first and then excess sucralose was added. The resultant mixtures were stirred at 30 °C for 6 h, during which the temperature was controlled by a thermostatical water bath with an accuracy of 0.05 K (DF-101S). The suspensions were held for 1 h, and HPLC measurements were executed on the supernatant. Each operation must be repeated three times; in detail, three supernatants in one sample were taken for HPLC measurements, and the uncertainty of mole fraction solubility must be lower than 0.5%.

2.5. X-ray Single Crystal Diffraction. Single crystals of sucralose have been crystallized in methanol and four antisolvents (IPN, IVD, IVA, and IBP). Diffraction intensity data were collected using a Bruker Apex Duo2 CCD area diffractometer equipped with a fine focus, 2.0 kW sealed tube X-ray source (Mo Kα radiation, λ = 0.71073 Å) at 293(2) K. Crystal structures were solved by the direct method with SHELXS and refined with the least-squares in SHELXL.[27] The final structures were verified by the ADDSYM algorithm in PLATON program.[28] Table S1 summarized all the refinement details in this work. Table S2 presents the important bond lengths and angles, and the hydrogen bonds are given in Table S3 [CCDC 2243495 and 2243497−2243500 contain the supplementary crystallographic data for this paper. These data can be obtained free of charge from The Cambridge Crystallographic Data Centre via www.ccdc.cam.ac.uk/data_request/cif.]

2.6. Theoretical Calculation Methods. The models of solvent−solvent interaction were constructed from GaussView 5.0 program, in which methanol···antisolvent interactions were based on their most possible hydrogen bonding sites. Then, geometry full optimizations have been conducted without constrained degrees of freedom using the spin restricted DFT method. The hybrid density functional B3LYP method and 6-31g(d) basis set was employed. The standard counterpoise method was applied to account for the basis set superposition errors (BSSE) for the calculations of energies. Their interaction energies were estimated according to the following equation: $\Delta E_{\text{int}} = E_{\text{AB}} - E_{\text{A}} - E_{\text{B}} + E_{\text{BSSE}}$, in which E_{BSSE} is BSSE energy. All DFT calculations were carried out using the Gaussian 09 package.[29]

https://doi.org/10.1021/acsomega.3c03877
ACS Omega 2023, 8, 41145−41155

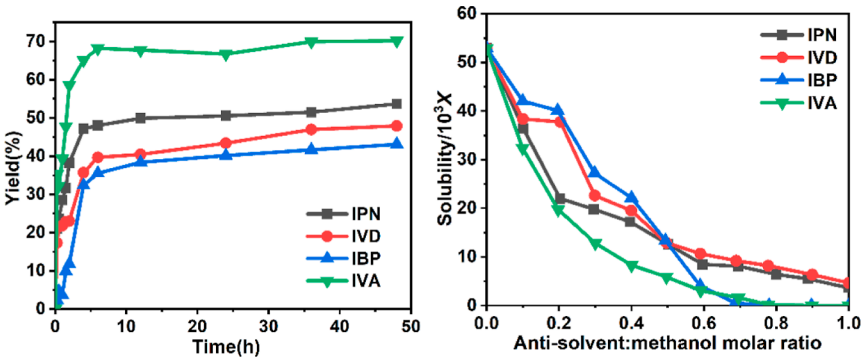

Figure 2. (a) Crystallizing rate measurement under different antisolvents; (b) the solubility of sucralose in methanol/antisolvent mixed solution with different molar ratio.

3. RESULTS AND DISCUSSION

3.1. Solvent Effect in Antisolvent Crystallization. Solvent effect is the most effective method in crystal morphology modulation.[30] Here, by fixing the solvent molar ratio, temperature, mass of crystal seed, and stirring rate, four antisolvents, i.e., IPN, IVD, IVA, and IBP were used to investigate the solvent effect in antisolvent crystallization of sucralose. First, the self-prepared sucralose was characterized by HPLC (Figure S1b). According to literature, the highest peak at 4.81 min can be attributed to the sucralose, other three weak peaks at 2.75, 3.26, and 3.42 min are assigned to the bis-chloro products, and the species at 7.03 min is 4,1′,6′-trichlorosucrose-6-acetate.[23,31] Its purity has been determined as 95.05% by the external standard method based on measurement of HPLC equipped with an RID detector (Figure S1b).

The antisolvent crystallization yields and purities at 24 and 48 h (methanol/antisolvent volume ratio of 1:1, 30 °C) can be seen in Figure 1a,b (their HPLC diagrams at 24 and 48 h can be found in Figure S1c,d). Four antisolvents can separate the sucralose from raw alcoholysis mixtures. At 24 h, the crystallization yield/purity are 34.38/97.34% (IVA), 16.54/97.58% (IPN), 16.3/96.33% (IVD), and 7.69/95.75% (IBP). When elongating the crystallizing time to 48 h, the corresponding parameters can be elevated as 49.33/97.61% (IVA), 36.45/97.65% (IPN), 29.31/96.33% (IVD), and 14.00/97.16% (IBP). Clearly, IVA exhibits the highest efficiency. Although the yield of 49.33% is relatively low, it is much higher than the yield of an industrial water-involved recrystallization process (27.33% for high purity sucralose, 7.17% for raw sucralose, Figure S2). We can further elongate the crystallizing time to obtain higher yield. The purity of 97.61% can be comparable to the traditional multiextraction and recrystallization process (about 98%, Figure S2). When using high-purity sucralose as starting material, much higher crystallization yield/purity can be achieved; for example, yield/purity of 68.21/99.98% at 12 h and 70.22/100% at 48 h can be found when using IVA as antisolvent (Figure 1c,d).

In the crystallizing rate measurement under different antisolvents, in order to exclude the effect of other byproducts, the high purity sucralose was used as starting material. The diagram of crystallizing rate using different antisolvents (IPN, IVD, IVA, and IBP) can be seen in Figure 2a. We have tried other ketone solvents as antisolvents, such as acetone, methylisobutyl ketone, and *N*-methyl-2-pyrrolidone, but no crystals were obtained. Therefore, compared with the functional groups including hydroxyl, formyl, carboxyl, and ester groups, the carbonyl of ketone is not an effective group for antisolvent crystallization of sucralose. When IPN, IVD, IVA, and IBP were used as antisolvents, the crystallizing rates reach to a maximum at 6 h for IVA and 12 h for the rest solvents. At the crystallizing time of 6 h, the yield using IVA can be as high as 68.21%, and the yield of 70.22% can be achieved at 48 h. At the same time, high purity can be realized (100%). However, much lower yields can be obtained using other three solvents (IPN 49.89%, IVD 40.45%, IBP 38.39% at 12 h, and IPN 53.66%, IVD 47.90%, and IBP 43.10% at 48 h). The crystallizing rate (defined as yield change in one h) order is IVA (5.64%/h) > IPN (4.16%/h) > IVD (3.37%/h) > IBP (3.20%/h) (crystallizing rate Figure 2a). The crystallizing rate can be further validated by sucralose solubility measurements in methanol/antisolvent mixed solvents with different molar ratios at 30 °C (Figure 2b). With the addition of antisolvents, the sucralose solubilities all decrease clearly, and the decreasing rate order is IVA > IPN > IVD > IBP. When the antisolvent molar ratio is 0.5 (i.e., methanol/antisolvent = 1:1), the sucralose solubility order is IVA < IPN < IVD < IBP, which is in agreement with the above crystallizing rate order. When the antisolvent molar ratio is 1, i.e., the solvents are pure antisolvents, the solubilities are very low. Specially, in pure IVA and IBP, the solubilities are close to zero. Ketone solvents do not work in ASC of sucralose. The factors including solvent−solvent interaction, solvent−solute interaction, and space confinement effect of solvents could affect the crystallization/dissolution of sucralose.[20] The insolubilities in pure antisolvents suggests that solvent−solute interactions play minor role in ASC of sucralose. The mechanism about the antisolvent crystallization will be discussed in the single crystal structures and theoretical section.

3.2. Characterizations and Properties of Sucralose by ASC Method. The products obtained from different antisolvent crystallizations were characterized by FT-IR, NMR, and XRD. As indicated by FT-IR spectra (Figure S3a), the peaks at 3460 and 3320 cm^{-1} stem from the stretching vibrations of hydroxyl groups. The vibrations at about 2930 cm^{-1} can be assigned to the stretching vibrations of methylene, and those in the range of 1480−1300 cm^{-1} are the bending vibrations of CH_2 and CH bonds. Specially, the peaks in the range of 1150−1000 cm^{-1} root from the stretching vibrations of C−OH and C−O−C on the skeleton, and C−Cl

https://doi.org/10.1021/acsomega.3c03877
ACS Omega 2023, 8, 41145−41155

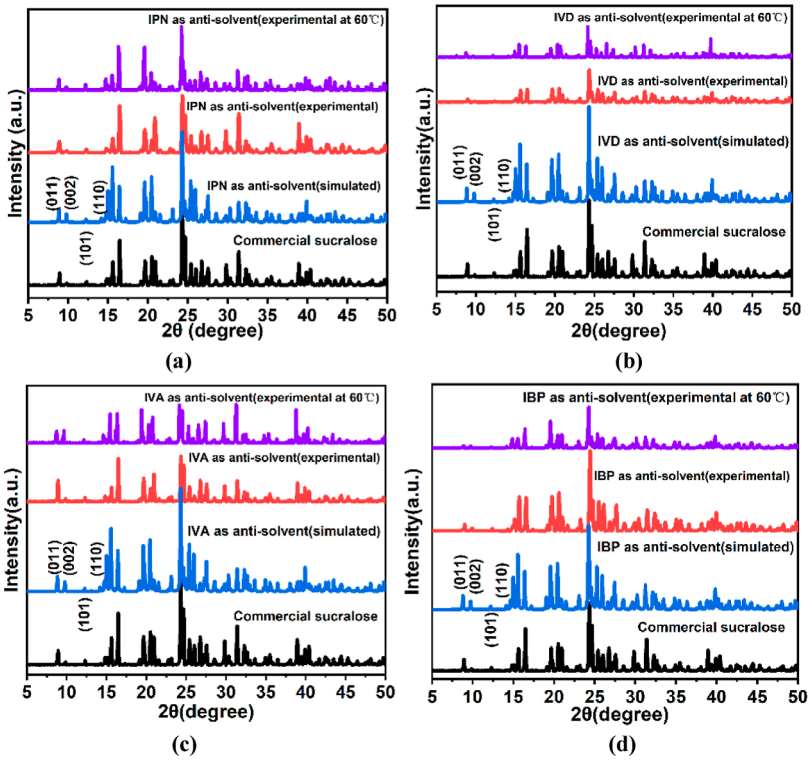

Figure 3. Simulated and experimental PXRD patterns of four sucralose products using different antisolvents: (a) IPN; (b) IVD; (c) IVA; and (d) IBP.

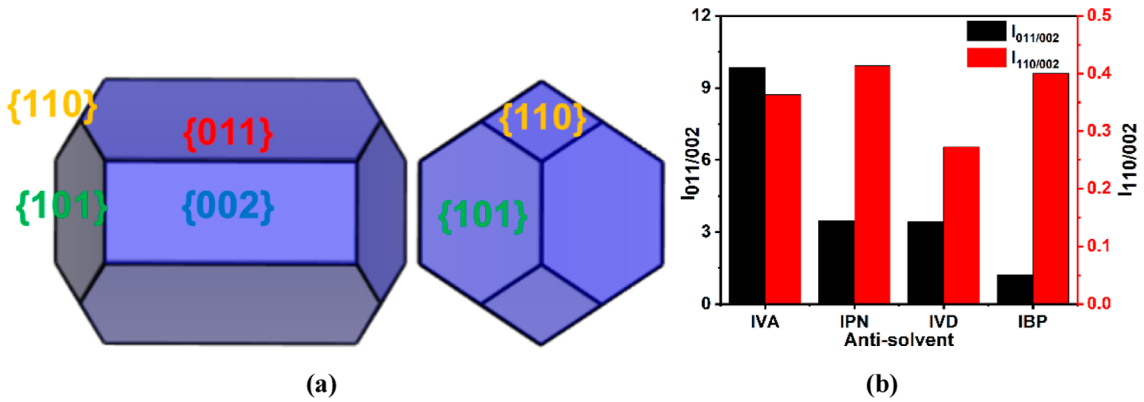

Figure 4. (a) Crystal faces based on attachment energy (AE) model; (b) strength ratio of different lattice planes deduced from PXRD patterns.

vibrations can be seen in 777−623 cm^{-1}.[32] The above zones are generally the same, but the −OH involved zones differ to some extent. In detail, the vibrations of −OH split into two peaks at about 3462 and 3320 cm^{-1}. The first ones are consistent with each other, but the latter range from 3322 to 3324 cm^{-1}, implying the difference in hydrogen bonding strengths. The chemical shifts of four products obtained from ASC methods are consistent with the commercially pure sucralose and literature (Figure S3b).[33]

XRD measurements were executed to probe the morphologies. As suggested by XRD diagrams, the experimental patterns obtained from antisolvent crystallizations and pure sucralose are consistent with the simulated ones based on single crystal structures, except that some diffraction intensities are different to some extent (Figure 3). Compared with the reported literature, no new crystalline phases appear in this work.[32,34] PXRD patterns at 60 °C are generally the same as those at room temperature, indicating that no phase transformations happened at these two temperatures. According to the simulated crystal faces based on attachment energy (AE) model, the needle morphology of sucralose includes four crystal faces, i.e., {011}, {002}, {101}, and {110} faces (Figure 4a).[22] Among these faces, {002} faces have the biggest facet area, and the facet area of the (110) face is the smallest. The growth rate order of these crystal faces has been determined as {110} > {101} > {011} > {002}, leading to their needle-like morphology. Besides, the lowest growth rate on {002} face is relative to the weaker intermolecular interactions along this face.[22] The strength ratio of different lattice planes can reflect the crystal preferred orientation.[35] The I_{011}/I_{002} order of four products using different antisolvents is IVA > IPN > IVD > IBP (Figure 4b). I_{011}/I_{002} of IVA (9.86) is three times higher than those of the others, and those of IPN and IVD differ little (3.44 and 3.40, respectively). However, all the I_{110}/I_{002} values

https://doi.org/10.1021/acsomega.3c03877
ACS Omega 2023, 8, 41145−41155

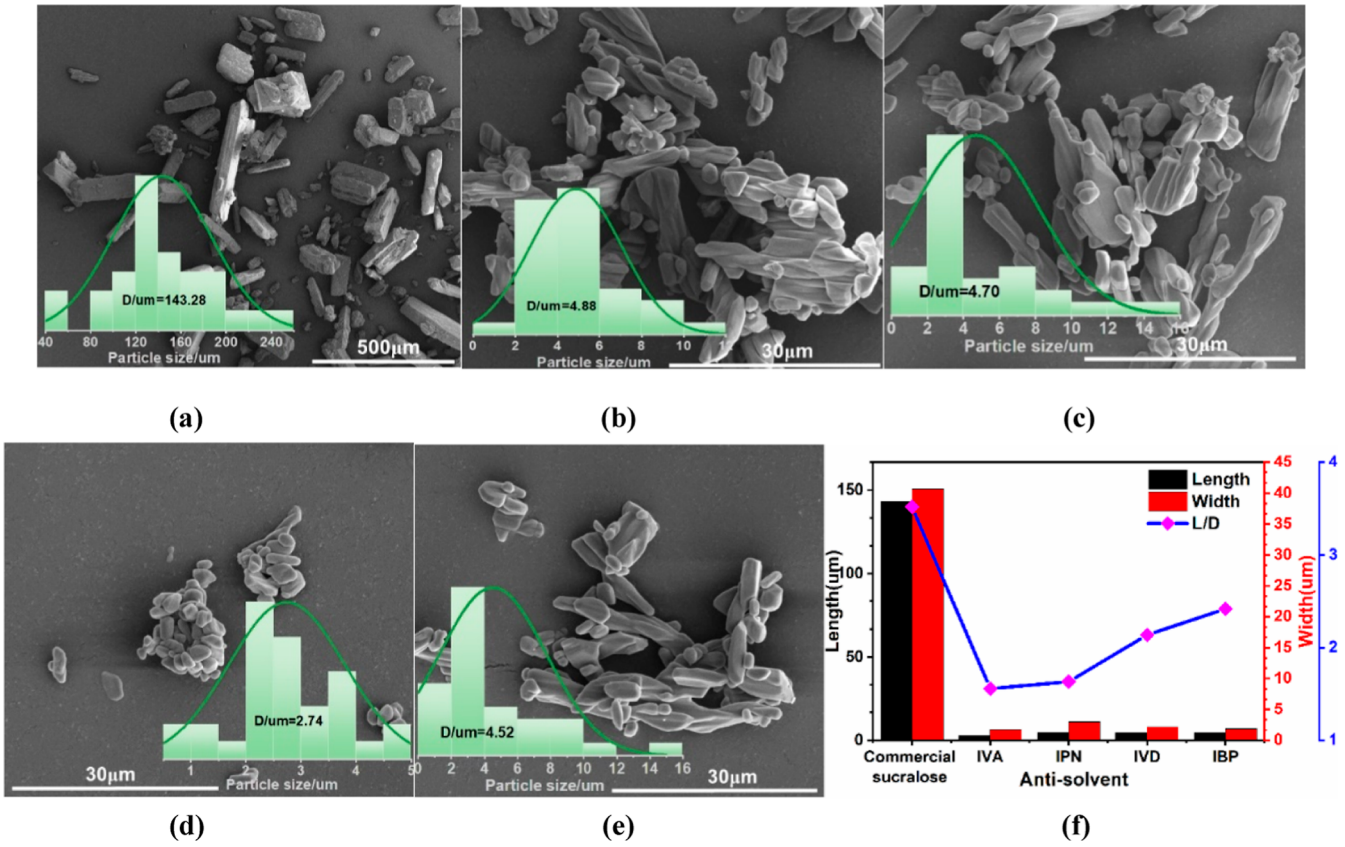

Figure 5. (a) SEM images of commercial sucralose and four sucralose products crystallized with different antisolvents showing the particle size distributions: (a) commercial sucralose; (b) IPN; (c) IVD; (d) IVA; (e) IBP; and (f) aspect ratio of sucralose products.

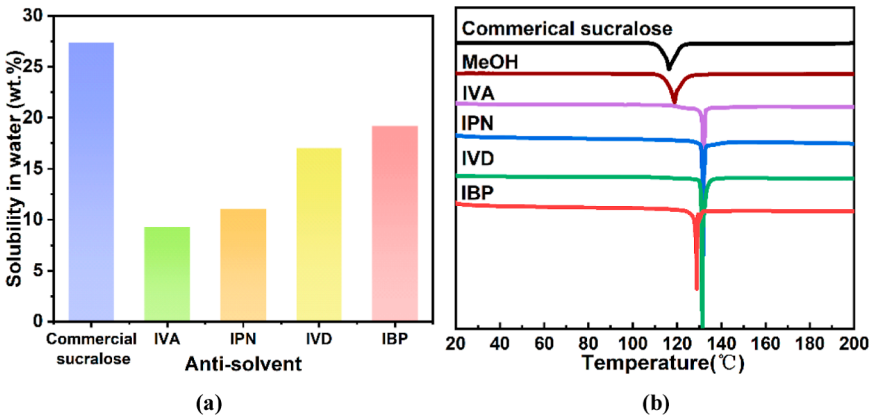

Figure 6. (a) Solubility in water at 30 °C. (b) DSC curves of four sucralose products crystallized with different antisolvents and commercially pure sucralose.

are much lower and fluctuate little (0.27−0.40). This character hints the products using IVA as antisolvent will possess the smallest aspect ratio.

The SEM images of four sucralose products crystallized with different antisolvents and commercial pure sucralose showing their particle size distributions are revealed in Figure 5. The commercial sucralose is needle-like crystals with a large size about 143.28 μm (Figure 5a). Sucralose obtained from ASC methods is also needle-like, but its sizes decrease sharply (IPN: 4.88 μm, IVD: 4.70 μm, IVA: 2.74 μm, IBP: 4.52 μm, Figure 5b−e). More importantly, after crystallizing with the ASC method, the aspect ratio of commercial sucralose decreases from 3.52 to 1.63 (IPN), 2.13 (IVD), 1.55 (IVA), and 2.41 (IBP) (Figure 5f). Clearly, sucralose product using IVA as antisolvent exhibits the smallest particle size and lowest aspect ratio, which is more spherical and will be beneficial for its further industrial handling.[22] Compared with the spherical product using mechanical grinding method, the particle size distributions of products under ASC method are more uniform.[36]

The solubilities of five kinds of sucraloses in water at 30 °C are plotted in Figure 6a. The solubility of commercially obtained sucralose is 27.38 wt %, which is generally consistent with the literature data of 26.94 and 28.00 wt %.[37,38] This consistency validates the reliability of our measurements. The solubilities of other products are 11.07 wt % (for IPN), 17.04

https://doi.org/10.1021/acsomega.3c03877
ACS Omega 2023, 8, 41145−41155

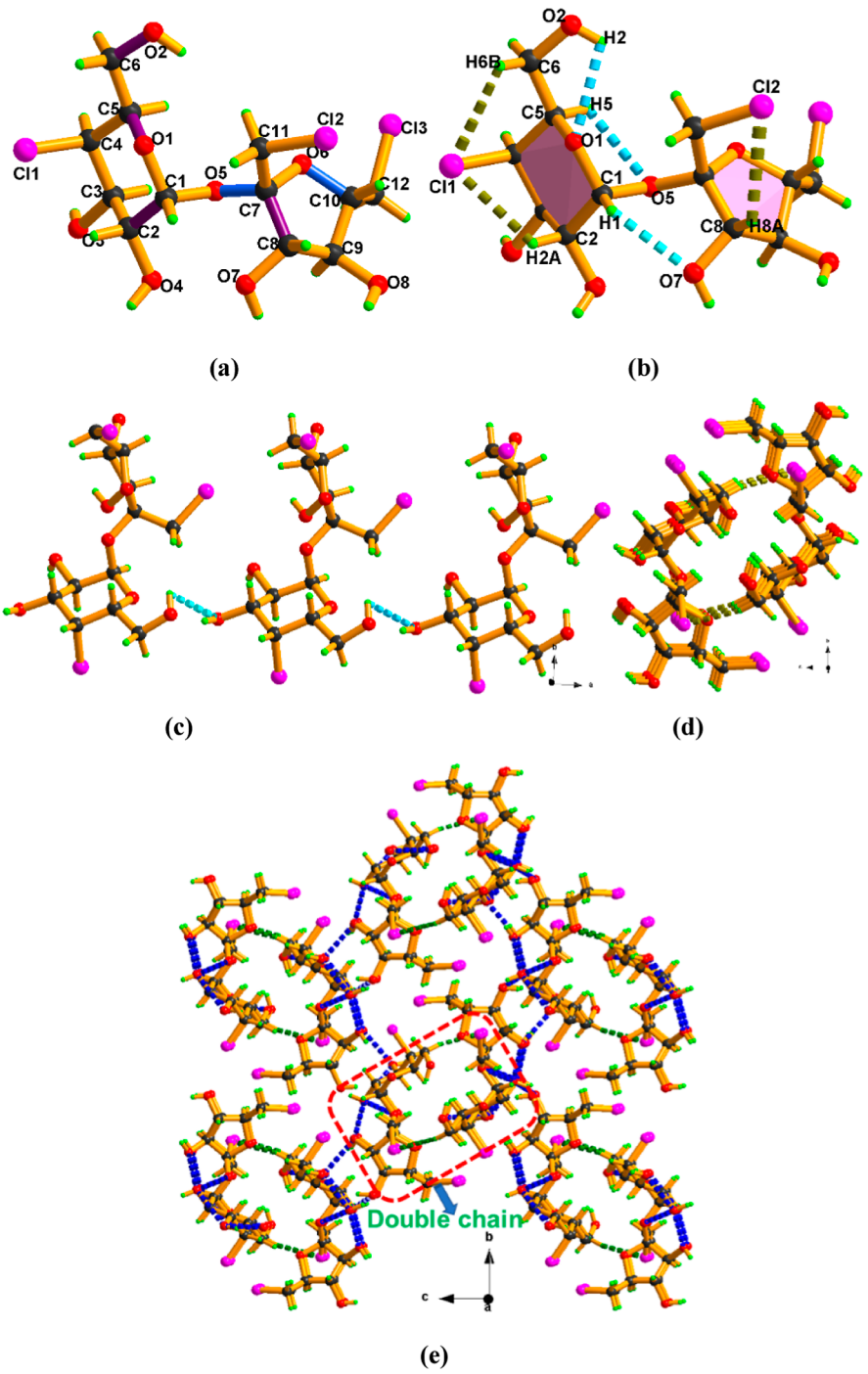

Figure 7. (a) Structure of sucralose using IVA as antisolvent; (b) the intramolecular hydrogen bonds; (c) the 1D chain via the O(3)−H(3)···O(2) hydrogen bond; (d) the double chain through the C(6)-H(6A)···Cl(2) hydrogen bond; and (e) 3D hydrogen bonding network of IVA.

wt % (for IVD), 9.28 wt % (for IVA), and 19.20 (for IBP) wt %, respectively. Clearly, the solubility of commercial sucralose is much higher than those of ASC-treated ones, which is due to its lower crystallinity. However, the ASC-treated products possess higher crystallinities, and some crystalline products are undissolved in water, which will decrease their solubilities. Besides, the lower solubilities might lead to higher affinity for binding neighboring hydrophobic interfaces.[9] Moreover, among the ASC-treated products, the IVA-treated one exhibits the lowest solubility. This trend could be assigned to the stronger intermolecular hydrogen bonding interactions in the lattice of IVA-treated product, which will be probed in the next single structural analysis. This character also implies its potential application in a special field such as sustained-release food or drugs.

Thermal stabilities of six kinds of sucraloses were determined by DSC measurement (Figure 6b). The DSC curve of commercial sucralose (T_{Onset}: 114.10 °C, T_{Peak}: 116.34 °C) fit well with literature,[32] which is assigned to the sucralose fusion, followed by its decomposition and release of water and hydrogen chloride.[39] The thermal behavior of sucralose recrystallized by methanol is as follows: T_{Onset}: 115.56 °C, T_{Peak}: 118.74 °C. The stabilities of sucraloses after ASC can be greatly elevated, in detail, IPN (T_{Onset}: 130.11 °C, T_{Peak}: 130.91

https://doi.org/10.1021/acsomega.3c03877
ACS Omega 2023, 8, 41145−41155

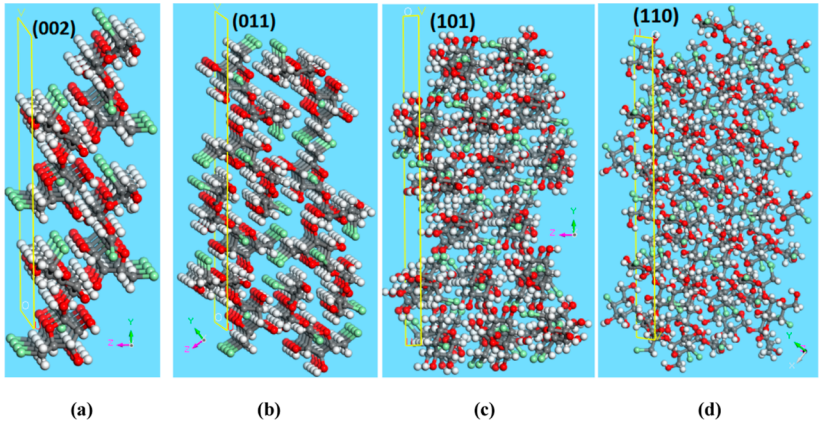

Figure 8. Four crystal faces of sucralose: (a) {002} face; (b) {011} face; (c) {101} face; and (d) {110} face.

°C), IVD (T_{Onset}: 130.91 °C, T_{Peak}: 131.01 °C), IVA (T_{Onset}: 131.40 °C, T_{Peak}: 131.65 °C), and IBP (T_{Onset}: 128.18 °C, T_{Peak}: 128.25 °C). Obviously, after the ASC process, the thermal stability of sucralose can be greatly enhanced. Because commercial sucralose is highly pure (Figure S1a), the effect of impurities on the thermal stability could be ruled out. Thus, the enhanced thermal stabilities could be led by stronger intermolecular interactions after ASC process. The IVA-treated one illustrates the best stability, stemming from the stronger C−H···Cl hydrogen bonds. The order of thermal stability agrees with that of solubility. Therefore, the ASC process is an efficient strategy for the improvement of sucralose stability, which can be very meaningful for the enhancement of biosafety or its postprocessing. In all, the ASC process can modulate the aspect ratio, solubility, and stability effectively. To our interest, when IVA is adopted as antisolvent, the highest separation efficiency, the smallest aspect ratio, the lowest solubility, and best stability can be achieved. The mechanism will be discussed based on the following crystal structure description and theoretical calculations.

3.3. Mechanism Study Based on Crystal Structures. In order to disclose the reason for the better morphology, solubility, and stability under different antisolvents, the single crystals of sucralose under traditional crystallization and ASC method were determined by X-ray single crystal diffraction. They all crystallize in the orthorhombic system with the $P2_12_12_1$ space group, whose structure has been previously reported.[34,40] In five structures, all the six-membered glucopyranosyl rings are in near ideal $^4C_1$ chair conformations, while the five-membered fructofuranosyl rings have $^4T_3$ conformation. The bond lengths of four sucraloses are generally the same, except that some C−C/C−O bonds in product using IVA as antisolvent differ clearly (Table S2). In detail, in the former four products, the C−C (1.473(14) ∼ 1.572(15) Å), C−O (1.400(11) ∼ 1.459(4) Å), and C−Cl (1.792(3) ∼ 1.810(3) Å) in two rings are all normal with single bond characters, which are consistent with literature.[40] Great difference can be seen in IVA-treated one, C(2)−C(3) (1.46(3) Å), C(7)−C(8) (1.51(3) Å), C(5)−O(1) (1.41(2) Å), and C(6)−O(2) (1.41(2) Å) are much shorter (purple bonds in Figure 7a); however, C(7)−O(5) (1.447(18) Å) and C(10)−O(6) (1.470(19) Å) are obviously longer (sky blue bonds in Figure 7a). About the conformation of glycosidic linkage, the C(1)−O(5)−C(7) angles are similar in the range of 117.74−119.28°. Specially, the C(1)−O(5)−C(7)−O(6) dihedral angles (−161.27−162.45°) are much larger than that of sucrose (−44.31°),[41] sucrose-6-acetate (−42.45°),[6] and sucrose-6-amide (−47.82°).[42] IVA-treated sucralose possesses the smallest C(1)−O(5)−C(7)−O(6) torsion angle of −161.27°. Therefore, compared with the conformation of free sucralose, the IVA-treated product exhibits great distortion, which will be stabilized by its stronger intermolecular interactions.

The most important issue is the hydrogen bonds, which can determine their physical performance, such as sweetness and solubility. Previous works have demonstrated that the molecular assembly and functionalities (fluorescence, phosphorescence, et al.) could be modulated by hydrogen bonds in cocrystals.[43−48] All the structures in this work are stabilized by versatile intra- or intermolecular hydrogen bonds. Here, the IVA-treated product was described as example. Six intramolecular hydrogen bonds (C/O−H···O, C−H···Cl, Table S6) are absent in IVA-treated sucralose, which is more versatile than reported ones (Figure 7b).[40] The adjacent sucralose molecules are linked into a 1D chain via an O(3)−H(3)···O(2) hydrogen bond along the *a*-axis (Table S6, Figure 7c), which are further connected into a double chain through a C(6)-H(6A)···Cl(2) hydrogen bond (Table S6 and Figure 7d). Finally, every double chain is connected with the neighboring four chains into a 3D network through four O−H···O hydrogen bonds (Table S6 and Figure 7e). The packing modes of the other four sucraloses are generally similar, except that the strengths of hydrogen bonds differ to some extent (Figure S4). In their intermolecular hydrogen bonds, the strength of C/O−H···O hydrogen bonds differ little, but those of C−H···Cl are different clearly. In detail, C···Cl distance of IVA-treated sucralose (3.715(4) Å) is shorter than other ones (3.743(17) ∼ 3.759(6) Å), giving rise to its lowest solubility. We have cleaved four crystal faces using the structure of IVA-treated sucralose as an example, as shown in Figure 8. Interestingly, on their {002} crystal surface, the impending bonds are all C−Cl bonds (Figure 8a). On {011}, the surface is dominated by C−Cl bonds with a small amount of O−H/C−H bonds (Figure 8b). However, on {101} and {110} faces, impending O−H/C−H bonds are dominant (Figure 8c,d). Thus, the stronger C−H···Cl hydrogen bonds in IVA-treated sucralose might be beneficial for the growth along {002}/{011} directions, which results in its lower aspect ratio. Besides, stronger C−H···Cl hydrogen bonds will inhibit its dissolution, giving rise to worse solubility.

The crystallization mechanism in the ASC process has been proposed as follows: (1) emulsion particles are generated upon

https://doi.org/10.1021/acsomega.3c03877
ACS Omega 2023, 8, 41145−41155

mixing two miscible liquids; (2) solute molecules are encapsulated among the emulsions, in which circular aggregates with small size can be formed without crystallinity. In this step, the shrinking of emulsion particle led by solvent escape can result in the supersaturation, which is very important to the nucleation; (3) with the increase of aggregate sizes, the crystallinity is elevated as well, and long-term order can be formed when the crystal facets are generated.[20] Based on this three-step mechanism, emulsion particles and confined-spaces defined by methanol/antisolvents can determine the morphologies and physical properties of sucralose products. Therefore, weak methanol···ketone interactions lead to their unavailability in ASC of sucralose.[20] It has been pointed out that solvent−solute interactions play a minor role in ASC of sucralose, so we focus the attention on the solvent−solvent interaction. We estimated the interactions between methanol and antisolvents by DFT calculations, whose geometries can be seen in Figure S5a−d. The emulsion binding strength can be defined by solvent···solvent interaction energy, and the higher binding strength means faster crystallization. The methanol··· antisolvent interaction energies are −4.14 kcal/mol (methanol···IPN), −4.51 kcal/mol (methanol···IVD), −10.60 kcal/mol (methanol···IVA), and −5.39 kcal/mol (methanol···IBP). The methanol···IVA emulsion possesses the strongest solvent−solvent interactions due to the presence of carboxyl group with hydrogen bonding donor and acceptor (Figure S5c), giving rise to the smallest spaces among the emulsions for nucleation. Consequently, the IVA-treated product exhibits the greatest distortion. Besides, the methanol···IVA interaction strength is twice that of other solvent−solvent ones. So, the formation of the emulsion will be accelerated, resulting in the fastest crystallizing rate. The other three interactions are close with each other, so the solvent escape will determine the crystallizing rate. The weaker interactions will be beneficial for the solvent escape and, as a result, the faster crystal growth speed. The methanol···MIBK interaction energy (−4.39 kcal/mol) can be comparable to that of methanol···IPN (Figure S5e). So, the unavailability of ketone solvents in sucralose ASC should be led by the presence of additional alkyl on MIBK, which can reduce the nucleation space.

4. CONCLUSIONS

In summary, we have successfully realized the simultaneous modulations of aspect ratio, solubility, and stability of sucralose using the ASC method in the alcoholysis process. In the four products using IPN, IVD, IVA, and IBP as antisolvents, the IVA-treated one possesses the highest separation efficiency, fastest crystallizing rate, lowest aspect ratio, lowest solubility, and best thermal stability. X-ray single crystal structure determinations suggest that IVA-treated sucralose exhibits the greatest molecular distortion and strongest intermolecular C−H···Cl hydrogen bonds, which will be beneficial for the crystal growth along {002}/{011} directions and the resultant lower aspect ratio. The strongest methanol···IVA interactions due to the presence of a carboxyl group can accelerate the formation of emulsion, resulting in the fastest crystallizing rate of the IVA-involved ASC process. This work is significant for the production of high-quality sucralose.

■ ASSOCIATED CONTENT

Supporting Information

The Supporting Information is available free of charge at https://pubs.acs.org/doi/10.1021/acsomega.3c03877.

Crystal data and structural determinations; selected bond lengths; hydrogen bonding details of this work; monogroup protection synthesis of sucralose from sucrose and the main bis- or monochloro byproducts in the alcoholysis reaction; HPLC diagrams of high-purity sucralose, self-prepared raw sucralose, and samples in antisolvent crystallization process at different times; yield and purity in traditional water-involved process; FT-IR spectra and NMR spectra of sucralose crystallized from different antisolvents; 3D hydrogen bonding network of sucraloses crystallized under different conditions; and the optimized geometries of methanol···antisolvents interactions (PDF)

Crystallographic data for IPN (CIF)

Crystallographic data for IVD (CIF)

Crystallographic data for IVA (CIF)

Crystallographic data for IBP (CIF)

Crystallographic data for methanol (CIF)

■ AUTHOR INFORMATION

Corresponding Authors

Yingshu Wang − *Fujian Engineering Research Center of Advanced Manufacturing Technology for Fine Chemicals, College of Chemical Engineering, Fuzhou University, Fuzhou 350108, P. R. China; Qingyuan Innovation Laboratory, Quanzhou 362801, P. R. China;* orcid.org/0000-0003-4448-0619; Email: ljhwysh@fzu.edu.cn

Huidong Zheng − *Fujian Engineering Research Center of Advanced Manufacturing Technology for Fine Chemicals, College of Chemical Engineering, Fuzhou University, Fuzhou 350108, P. R. China; Qingyuan Innovation Laboratory, Quanzhou 362801, P. R. China;* orcid.org/0000-0002-8346-7284; Email: youngman@fzu.edu.cn

Authors

Qiaoyan Xu − *Fujian Engineering Research Center of Advanced Manufacturing Technology for Fine Chemicals, College of Chemical Engineering, Fuzhou University, Fuzhou 350108, P. R. China; Qingyuan Innovation Laboratory, Quanzhou 362801, P. R. China*

Zhoulin Lv − *College of Chemistry, Fuzhou University, Fuzhou 350108, P. R. China*

Xiaoping Chen − *Fujian Engineering Research Center of Advanced Manufacturing Technology for Fine Chemicals, College of Chemical Engineering, Fuzhou University, Fuzhou 350108, P. R. China; Qingyuan Innovation Laboratory, Quanzhou 362801, P. R. China*

Shaoheng Li − *Fujian Engineering Research Center of Advanced Manufacturing Technology for Fine Chemicals, College of Chemical Engineering, Fuzhou University, Fuzhou 350108, P. R. China; Qingyuan Innovation Laboratory, Quanzhou 362801, P. R. China*

Changqi Huang − *Fujian Engineering Research Center of Advanced Manufacturing Technology for Fine Chemicals, College of Chemical Engineering, Fuzhou University, Fuzhou 350108, P. R. China; Qingyuan Innovation Laboratory, Quanzhou 362801, P. R. China*

Jingjing Chen − *Fujian Engineering Research Center of Advanced Manufacturing Technology for Fine Chemicals, College of Chemical Engineering, Fuzhou University, Fuzhou 350108, P. R. China; Qingyuan Innovation Laboratory, Quanzhou 362801, P. R. China*

https://doi.org/10.1021/acsomega.3c03877
ACS Omega 2023, 8, 41145−41155

Haohong Li − *Fujian Engineering Research Center of Advanced Manufacturing Technology for Fine Chemicals, College of Chemical Engineering, Fuzhou University, Fuzhou 350108, P. R. China; College of Chemistry, Fuzhou University, Fuzhou 350108, P. R. China;* orcid.org/0000-0003-3543-7715

Complete contact information is available at: https://pubs.acs.org/10.1021/acsomega.3c03877

Notes

The authors declare no competing financial interest.

■ ACKNOWLEDGMENTS

This study was financial supported by Key Program of Qingyuan Innovation Laboratory (grant no. 00221001), the National Natural Science Foundation of China (no. 22078065), and Quanzhou Science and Technology Program Project (no. 2020C008R).

■ REFERENCES

(1) Mora, M. R.; Dando, R. The Sensory Properties and Metabolic Impact of Natural and Synthetic Sweeteners. *Rev. Food Sci. Food Saf.* **2021**, *20*, 1554−1583.
(2) Chappell, G. A.; Wikoff, D. S.; Doepker, C. L.; Borghoff, S. J. Lack of potential carcinogenicity for acesulfame potassium − Systematic evaluation and integration of mechanistic data into the totality of the evidence. *Food Chem. Toxicol.* **2020**, *141*, 111375.
(3) Grotz, V. L.; Munro, I. C. An Overview of the Safety of Sucralose. *Regul. Toxicol. Pharmacol.* **2009**, *55*, 1−5.
(4) Luo, Y.; Xu, L.; Sun, X. Synthesis of Strong Sweetener Sucralose. *Mod. Appl. Sci.* **2008**, *2*, 13−15.
(5) Ferrer, M.; Cruces, M. A.; Bernabé, M.; Ballesteros, A.; Plou, F. J. Lipase-catalyzed Regioselective Acylation of Sucrose in Two-solvent Mixtures. *Biotechnol. Bioeng.* **1999**, *65*, 10−16.
(6) Chen, X.; Li, S.; Xu, Q.; Chen, Z. R.; Lin, S.; Yan, Z.; Chen, J.; Li, H.; Zheng, H. Selective Co-crystallization Separation of Sucrose-6-acetate from Complicated Sucrose Acylation System and Facile Removal of Co-former: Process Optimizations and Mechanisms. *Sep. Purif. Technol.* **2022**, *301*, 122027.
(7) Chen, M.; Yu, C.; Yao, M.; Liu, X.; Xu, S.; Tang, W.; Dong, W.; Gong, J. The Time and Location Dependent Prediction of Crystal Caking by a Modified Crystal Bridge Growth Model and DEM Simulation Considering Particle Size and Shape. *Chem. Eng. Sci.* **2020**, *214*, 115419.
(8) Silva, C.; Santos, J.; Melia Rodrigo, M.; Ribeiro, A.; Valente, A.; Abreu, P. E.; Marques, J.; Esteso, M. A. On the Transport and Dynamics of Disaccharides: H-bonding Effect in Sucrose and Sucralose. *J. Mol. Liq.* **2022**, *345*, 117855.
(9) Shukla, N.; Pomarico, E.; Hecht, C. J. S.; Taylor, E. A.; Chergui, M.; Othon, C. M. Hydrophobic Interactions of Sucralose with Protein Structures. *Arch. Biochem. Biophys.* **2018**, *639*, 38−43.
(10) de Oliveira, D. N.; de Menezes, M.; Catharino, R. R. Thermal Degradation of Sucralose: A Combination of Analytical Methods to Determine Stability and Chlorinated by Products. *Sci. Rep.* **2015**, *5*, 9598.
(11) Kozhummal, R.; Yang, Y.; Güder, F.; Küçükbayrak, U. M.; Zacharias, M. Antisolvent Crystallization Approach to Construction of CuI Superstructures with Defined Geometries. *ACS Nano* **2013**, *7*, 2820−2828.
(12) Mostafa Nowee, S.; Abbas, A.; Romagnoli, J. A. Antisolvent Crystallization: Model Identification, Experimental Validation and Dynamic Simulation. *Chem. Eng. Sci.* **2008**, *63*, 5457−5467.
(13) Madane, K.; Ranade, V. V. Anti-solvent Crystallization: Particle Size Distribution with Different Devices. *Chem. Eng. J.* **2022**, *446*, 137235.
(14) Coquerel, G. Crystallization of Molecular Systems from Solution: Phase Diagrams, Supersaturation and Other Basic Concepts. *Chem. Soc. Rev.* **2014**, *43*, 2286−2300.
(15) Schall, J. M.; Capellades, G.; Myerson, A. S. Methods for Estimating Supersaturation in Antisolvent Crystallization Systems. *CrystEngComm* **2019**, *21*, 5811−5817.
(16) Kim, J.; Park, C.; Choi, H. C. Selective Growth of a C_{70} Crystal in a Mixed Solvent System: From Cube to Tube. *Chem. Mater.* **2015**, *27*, 2408−2413.
(17) Huang, L.; Liao, Q.; Shi, Q.; Fu, H.; Ma, J.; Yao, J. Rubrene Micro-Crystals from Solution Routes: Their Crystallography, Morphology and Optical Properties. *J. Mater. Chem.* **2010**, *20*, 159−166.
(18) Park, Y.; Koo, J. Y.; Choi, H. C. Additive-Free Morphology Control of Organic Polyhedral Molecular Crystals by the Antisolvent Molecular Geometry: From Rod, Disk, to Cube. *Cryst. Growth Des.* **2018**, *18*, 7239−7243.
(19) Liu, D. D.; Yu, N. S.; Liu, D. P.; He, Y. Y.; Liu, R.; Li, Q. J.; Liu, B.; Liu, B. B. The Effect of Trichlorobenzene Solvent Geometry on the Morphologies of C60 Nano/microcrystals Produced from Solution. *Mater. Res. Bull.* **2016**, *73*, 65−69.
(20) Park, Y.; Song, K.; Choi, H. C. Emulsions of Miscible Solvents: the Origin of Antisolvent Crystallization. *CrystEngComm* **2021**, *23*, 777−782.
(21) Zhong, X.; Huang, C.; Chen, L.; Yang, Q.; Huang, Y. Effect of Ultrasound on the Kinetics of Anti-Solvent Crystallization of Sucrose. *Ultrason. Sonochem.* **2022**, *82*, 105886.
(22) Cui, P.; Yin, Q.; Zhang, S.; Cheng, X.; Dai, J.; Zhang, Z.; Zhou, L.; Xie, C. The Effect of Solvents on Crystal Morphology of Sucralose: Experiments and Molecular Dynamics Simulation Studies. *J. Cryst. Growth* **2020**, *532*, 125398.
(23) Yan, W.; Wang, N.; Zhang, P.; Zhang, J.; Wu, S.; Zhu, Y. Analysis of Sucrose Acetates in a Crude 6-O-acetyl Sucrose Product by On-line Hydrolysis-high-performance Liquid Chromatography with Pulsed Amperometric Detection. *J. Chromatogr. A* **2016**, *1449*, 71−77.
(24) Mufti, K. S.; Khan, R. A. Process for the Preparation of 4,1',6'-trichloro-4,1',6'-Trideoxygalactosucrose (TGS). U.S. Patent 4,380,476 A, 1983.
(25) Khan, R. A.; Mufti, K. S.; Patel, G. D. Trichloro, 6-substituted Sucrose Compounds, Compositions and uses Therefor. U.S. Patent 4,612,373 A, 1986.
(26) Gan, L. S.; Wang, Z. Z.; Zhou, C. X. Solubility of Podophyllotoxin in Six Organic Solvents from (283.2 to 323.2) K. *Chem. Eng. Data* **2009**, *54*, 160−161.
(27) Sheldrick, G. M. A Short History of SHELX. *Acta Crystallogr., Sect. A* **2008**, *64*, 112−122.
(28) Spek, A. L. Single-crystal Structure Validation with the Program PLATON. *J. Appl. Crystallogr.* **2003**, *36*, 7−13.
(29) Frisch, M. J.; Trucks, G. W.; Schlegel, H. B.; Scuseria, G. E.; Robb, M. A.; Cheeseman, J. R.; Scalmani, G.; Barone, V.; Mennucci, B.; Patersson, G. A. *Gaussian 09*. Revision A.1; Gaussian Inc: Petersson, 2009.
(30) Nguyen, T. T. H.; Rosbottom, I.; Marziano, I.; Hammond, R. B.; Roberts, K. J. Crystal Morphology and Interfacial Stability of RS-Ibuprofen in Relation to Its Molecular and Synthonic Structure. *Cryst. Growth Des.* **2017**, *17*, 3088−3099.
(31) Yan, W.; Wang, N.; Zhang, P.; Zhang, J.; Wu, S.; Zhu, Y. Simultaneous Determination of Sucralose and Related Compounds by High-performance Liquid Chromatography with Evaporative Light Scattering Detection. *Food Chem.* **2016**, *204*, 358−364.
(32) Aldeeb, O. A. A.; Mahgoub, H.; Foda, N. H. Sucralose. *Profiles Drug Subst., Excipients, Relat. Methodol.* **2013**, *38*, 423−462.
(33) Jung, M. H.; Kim, H. S.; Ahn, S.; Kim, S. T.; Jin, M. H.; Yim, Y. H.; Kim, Y. K.; Ok, J. H. Complete Assignment of the ^{1}H and ^{13}C NMR Spectra of a Sucrose Ester from Euphorbia Lathyris L. *J. Korean Magn. Reson.* **2000**, *4*, 125−132.
(34) Kanters, J. A.; Scherrenberg, R. L.; Leeflang, B. R.; Kroon, J.; Mathlouthi, M. The Crystal and Molecular Structure of An Intensely

Sweet Chlorodeoxysucrose; 4,1′,6′-trichloro-4,1′,6′-trideoxy-galacto-sucrose. *Carbohydr. Res.* **1988**, *180*, 175−182.
(35) Zhou, H.; Feng, M.; Song, K.; Liao, B.; Wang, Y.; Liu, R.; Gong, X.; Zhang, D.; Cao, L.; Chen, S. A Highly [001]-Textured Sb_2Se_3 Photocathode for Efficient Photoelectrochemical Water Reduction. *Nanoscale* **2019**, *11*, 22871−22879.
(36) Yang, Y.; Song, L.; Gao, T.; Nagy, Z. K. Integrated Upstream and Downstream Application of Wet Milling with Continuous Mixed Suspension Mixed Product Removal Crystallization. *Cryst. Growth Des.* **2015**, *15*, 5879−5885.
(37) Jora, M. Z.; da Silva Barbosa, M.; de Alencar Simoni, J.; Sabadini, E. Solubility and Molar Enthalpy of Solution of Sucralose in H_2O and D_2O. *Fluid Phase Equilib.* **2018**, *460*, 45−50.
(38) Li, X.; Du, Z.; Huang, X.; Yuan, W.; Ying, H. Solubility of Sucralose in Different Solvents from (283.15 to 333.15) K. *J. Chem. Eng. Data* **2010**, *55*, 2600−2602.
(39) Lv, N.; Guo, T.; Liu, B.; Wang, C.; Singh, V.; Xu, X.; Li, X.; Chen, D.; Gref, R.; Zhang, J. Improvement in Thermal Stability of Sucralose by γ-Cyclodextrin Metal-Organic Frameworks. *Pharm. Res.* **2017**, *34*, 269−278.
(40) Linden, A.; Muhammad Sofian, A. S.; Lee, C. K. 2,3,3′,6-Tetra-*O*-acetyl-4,1′,6′-trichloro-4,1′,4′,6′-tetradeoxygalactosucrose. *Acta Crystallogr.* **2002**, *58*, o718−o720.
(41) Jaradat, D. M. M.; Mebs, S.; Chęcińska, L.; Luger, P. Experimental Charge Density of Sucrose at 20 K: Bond Topological, Atomic, and Intermolecular Quantitative Properties. *Carbohydr. Res.* **2007**, *342*, 1480−1489.
(42) Fujimoto, T.; Nishio, T.; Hosaka, H.; Mizoguchi, S.; Tashiro, M. Crystal Structure of β-D-Fructofuranosyl-[2↔1]-6-amido-6-deoxy-α-D-glucopyranoside. *X-ray Struct. Anal. Online* **2017**, *33*, 63−64.
(43) Yan, D.; Jones, W.; Fan, G.; Wei, M.; Evans, D. G. Organic Microbelt Array Based on Hydrogen-bond Architecture Showing Polarized Fluorescence and Two-photon Emission. *J. Mater. Chem. C* **2013**, *1*, 4138−4145.
(44) Zhou, B.; Zhao, Q.; Tang, L.; Yan, D. Tunable Room Temperature Phosphorescence and Energy Transfer in Ratiometric Co-crystals. *Chem. Commun.* **2020**, *56*, 7698−7701.
(45) Zhou, B.; Yan, D. Hydrogen-Bonded Two-Component Ionic Crystals Showing Enhanced Long-Lived Room-Temperature Phosphorescence via TADF-Assisted Foster Resonance Energy Transfer. *Adv. Funct. Mater.* **2019**, *29*, 1807599.
(46) Li, S.; Lin, Y.; Yan, D. Two-component Molecular Cocrystals of 9-acetylanthracene with Highly Tunable One-/two-photon Fluorescence and Aggregation Induced Emission. *J. Mater. Chem. C* **2016**, *4*, 2527−2534.
(47) Lu, B.; Liu, S.; Yan, D. Recent Advances in Photofunctional Polymorphs of Molecular Materials. *Chin. Chem. Lett.* **2019**, *30*, 1908−1922.
(48) Yan, D. Micro-/Nanostructured Multicomponent Molecular Materials: Design, Assembly, and Functionality. *Chem.—Eur. J.* **2015**, *21*, 4880−4896.

https://doi.org/10.1021/acsomega.3c03877
ACS Omega 2023, 8, 41145−41155